Passive Intermodulation on Microstrip Lines

Dmitry Zelenchuk[#1], Aleksey P. Shitvov[#2], Alex G. Schuchinsky[#3], Torbjörn Olsson[*4]

[#]*ECIT, Queen's University of Belfast, Queen's Road, Queen's Island, Belfast, UK*

[1]d.zelenchuk@qub.ac.uk, [2]a.shitvov@queens-belfast.ac.uk, [3]a.schuchinsky@qub.ac.uk

[*]*Powerwave Technologies, Sweden*

[4]Torbjorn.Olsson@pwav.com

***Abstract*— The theory of passive intermodulation generation on printed transmission lines has been proposed. The new model for a terminated section of the transmission line with distributed nonlinear resistance has been developed and verified against the published experimental data. The closed form relation between the macroscopic nonlinear resistance and microscopic nonlinear surface resistivity of strip conductors has been obtained for microstrip lines. Effects of microstrip line width, length and matching on passive intermodulation generation have been studied in detail.**

I. Introduction

Passive intermodulation (PIM) is notoriously known for its detrimental effect on performance of base stations used in the space, military and civil telecommunications [1], [2]. PIM products, resulting from nonlinear frequency mixing by passive devices, occur in the reception band of antenna and degrade the system signal integrity. Printed circuit boards (PCBs) are nowadays perceived as one of the contributors into the PIM performance of the RF front end. Also, an increasing use of PCB based packaged devices in the high power applications imposes even more stringent requirements onto PIM performance of printed lines [3], [4], [5].

The recent studies reported that the copper grade, roughness, finishing and other laminate properties can significantly affect PIM characteristics of PCB [6], [7]. These observations indicated that PIM sources are associated with the distributed current-driven nonlinearity of printed conductors. Since the PIM products are usually measured at the level about 100dBc below the carrier signal [4], [5], [6], the nonlinearity observed in PCB is weak and manifests itself as the second order effect as compared to the insertion loss.

The existing PIM models are based on the assumption that PIM products are generated by lumped sources, cf. e.g. [3]. However, such an approach is hardly applicable to microstrip traces, and an alternative model is necessary to elucidate PIM mechanisms on PCB. To address the problem of distributed PIM generation, a new model is proposed here for a finite section of the terminated microstrip transmission line with distributed weakly nonlinear resistance, which is determined by the microscopic nonlinear surface resistivity of conductors. The proposed model and the analysis procedure are described in Section II. In Section III, the relationships between macroscopic and microscopic nonlinear parameters for a microstrip line are detailed. The results of the model verification and analysis of the effects of microstrip line parameters (width, length and termination load) on the PIM characteristics are presented in Section IV.

II. Problem Statement and Solution

A section of the transmission line of length l with weakly nonlinear impedance Z (Fig.1) is excited by the two-tone source with voltage amplitude V_0 and impedance Z_S. The other end of the line is terminated in the load with impedance Z_L. Assuming that the nonlinearity is associated with the distributed nonlinear resistance $R(I)$, waves on the transmission line are described by the nonlinear telegrapher's equations for current $I(x,t)$ and voltage $U(x,t)$ [8]

$$\begin{aligned}\frac{\partial I(x,t)}{\partial x} &= -\left(C\frac{\partial U(x,t)}{\partial t} + GU(x,t)\right)\\ \frac{\partial U(x,t)}{\partial x} &= -\left(L\frac{\partial I(x,t)}{\partial t} + R(I)I(x,t)\right)\end{aligned} \tag{1}$$

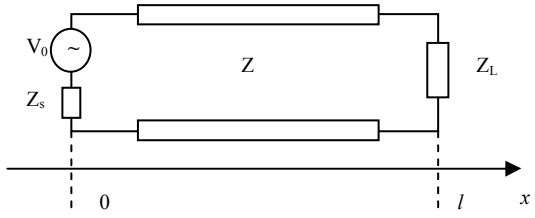

Fig. 1. Section of nonlinear microstrip line.

Here we consider only the third order intermodulation products, but the higher order products can be obtained in the same fashion. Therefore, the nonlinear resistance can be approximated as follows

$$R(I) = R_0 + R_2 I^2 \tag{2}$$

and the closed-form expressions for per-unit-length parameters C, G, L, R_0 of the canonical transmission lines can be found, for example, in [8].

Substituting (2) into (1) results in the nonlinear equation for the current distribution on the line

$$\begin{aligned}&\frac{\partial^2 I(x,t)}{\partial x^2} - \left(CL\frac{\partial^2 I(x,t)}{\partial t^2} + (CR_0 + GL)\frac{\partial I(x,t)}{\partial t} + GR_0 I(x,t)\right) =\\ &= R_2 I^2(x,t)\left(3C\frac{\partial I(x,t)}{\partial t} + GI(x,t)\right)\end{aligned} \tag{3}$$

For a weak nonlinearity, the steady-state solution of (3) can be obtained by the perturbation analysis in the form

$$I(x,t) = \sum_{k=0}^{\infty}\sum_{q=-\infty}^{\infty}\sum_{p=-\infty}^{\infty} R_2^k I_{q,p,k}(x)\exp(i\omega_{q,p}t) \tag{4}$$

where $\omega_{q,p} = q\omega_1 + p\omega_2$; ω_1, ω_2 are angular frequencies of carriers and $R_2^k I_{q,p,k}(x)$ is the k^{th} order perturbation term in the current expansion at a frequency harmonic $\omega_{q,p}$. It is necessary to note that the number of harmonics contributing to the k^{th} approximation in (4) is determined by the perturbation order k. The selection rule requires only the terms $I_{q,p,k}(x)$ with indices

$$|q| + |p| = 2d + 1, d \in [0, k] \tag{5}$$

be nonzero.

Using the series (4) and collecting the terms for each frequency harmonic and power of R_2, the nonlinear equation (3) can be written as follows

$$\left(\frac{d^2}{dx^2} - \gamma_{q,p}^2\right) I_{q,p,k}(x) = \tag{6}$$

$$= \sum_{v=0}^{k-1} \sum_{j=0}^{v} \sum_{m=-\infty}^{\infty} \sum_{n=-\infty}^{\infty} \sum_{r=-\infty}^{\infty} \sum_{s=-\infty}^{\infty} \left(3i\omega_{q-r,p-s}C + G\right) I_{m,n,j}(x) I_{r-m,s-n,v-j}(x) I_{q-r,p-s,k-v-1}(x)$$

The respective boundary conditions of the current and voltage continuity at $x=0$ and $x=l$ take the form

$$V_{0\,q,p}\delta_{0,k} - Z_s(\omega_{q,p}) I_{q,p,k}(0) = -\frac{1}{i\omega_{q,p}C + G} \frac{dI_{q,p,k}}{dx}\Big|_{x=0}$$

$$Z_L(\omega_{q,p}) I_{q,p,k}(l) = -\frac{1}{i\omega_{q,p}C + G} \frac{dI_{q,p,k}}{dx}\Big|_{x=l}$$

where $\gamma_{q,p}$ is the complex propagation constant [8], $V_{0\,q,p}$ - complex Fourier amplitudes of the source signal and $\delta_{0,k}$ - Kronecker delta. Thus, the nonlinear equation (3) has been reduced to the system of inhomogeneous linear equations (6). Then for perturbation of the 1st order, the third order intermodulation current can be represented as follows

$$I_{q,p,1}(x) = A_{q,p,1} \exp(-\gamma_{q,p} x) + B_{q,p,1} \exp(-\gamma_{q,p}(l - x)) + F_{q,p,1}(x) \tag{7}$$

where

$$A_{q,p,1} = \frac{1}{D_{q,p}} \left(\frac{S_{q,p}}{Z_S(\omega_{q,p}) + Z(\omega_{q,p})} - \frac{u_{q,p} Q_{q,p} \Gamma_S(\omega_{q,p})}{Z_L(\omega_{q,p}) + Z(\omega_{q,p})} \right),$$

$$B_{q,p,1} = \frac{1}{D_{q,p}} \left(\frac{Q_{q,p}}{Z_L(\omega_{q,p}) + Z(\omega_{q,p})} - \frac{u_{q,p} S_{q,p} \Gamma_L(\omega_{q,p})}{Z_S(\omega_{q,p}) + Z(\omega_{q,p})} \right),$$

$$u_{q,p} = \exp(-\gamma_{q,p} l),\ D_{q,p} = 1 - \Gamma_L(\omega_{q,p}) \Gamma_s(\omega_{q,p}) u_{q,p}^2,$$

$$S_{q,p} = Z_s(\omega_{q,p}) F_{q,p,1}(0) - Z(\omega_{q,p}) \Psi_{q,p,1}(0),$$

$$Q_{q,p} = -\left(Z(\omega_{q,p}) \Psi_{q,p,1}(l) + Z_L(\omega_{q,p}) F_{q,p,1}(l)\right),$$

$\Psi_{q,p,1}(x) = \dfrac{1}{\gamma_{q,p}} \dfrac{dF_{q,p,1}(x)}{dx}$, $\Gamma_L(\omega_{q,p})$, $\Gamma_S(\omega_{q,p})$ – the load and source reflection coefficients [8].

The part of (7), corresponding to inhomogeneous solution, $F_{q,p,1}(x)$ is unique for each harmonic and depends on amplitudes of the linear solution:

$$A_{r,s,0} = \frac{V_{0\,r,s}}{D_{r,s}\left(Z_s(\omega_{r,s}) + Z(\omega_{r,s})\right)},\ B_{r,s,0} = -\frac{\Gamma_L(\omega_{r,s}) V_{0\,r,s} u_{r,s}}{D_{r,s}\left(Z_s(\omega_{r,s}) + Z(\omega_{r,s})\right)}$$

where r and s satisfy (5) at $k = 0$.

The closed form expression for this function has been obtained for each harmonic that is sufficient for evaluation of the third order intermodulation products. For the sake of brevity, only the function $F_{2,-1,1}(x)$ for the harmonic frequency $\omega_{2,-1}$ is considered here as a representative example, and all the results of the PIM simulations presented below are calculated at this frequency:

$$F_{2,-1,1}(x) = 3\left(G + i\omega_{2,-1}C\right) \times$$

$$\times \left(\begin{array}{l} \dfrac{A_{1,0,0}^2 A_{0,-1,0} \exp\left(-\left(2\gamma_{1,0} + \gamma_{0,-1}\right)x\right)}{\left(2\gamma_{1,0} + \gamma_{0,-1}\right)^2 - \gamma_{2,-1}^2} + \\ + \dfrac{A_{1,0,0}^2 B_{0,-1,0} \exp\left(-\left(2\gamma_{1,0} - \gamma_{0,-1}\right)x - \gamma_{0,-1} l\right)}{\left(2\gamma_{1,0} - \gamma_{0,-1}\right)^2 - \gamma_{2,-1}^2} + \\ + \dfrac{2 A_{1,0,0} B_{1,0,0} A_{0,-1,0} \exp\left(-\gamma_{0,-1} x - \gamma_{1,0} l\right)}{\gamma_{0,-1}^2 - \gamma_{2,-1}^2} + \\ + \dfrac{2 A_{1,0,0} B_{1,0,0} B_{0,-1,0} \exp\left(\gamma_{0,-1} x - \left(\gamma_{1,0} + \gamma_{0,-1}\right) l\right)}{\gamma_{0,-1}^2 - \gamma_{2,-1}^2} + \\ + \dfrac{B_{1,0,0}^2 A_{0,-1,0} \exp\left(\left(2\gamma_{1,0} - \gamma_{0,-1}\right)x - 2\gamma_{1,0} l\right)}{\left(2\gamma_{1,0} - \gamma_{0,-1}\right)^2 - \gamma_{2,-1}^2} + \\ + \dfrac{B_{1,0,0}^2 B_{0,-1,0} \exp\left(\left(2\gamma_{1,0} + \gamma_{0,-1}\right)(x - l)\right)}{\left(2\gamma_{1,0} + \gamma_{0,-1}\right)^2 - \gamma_{2,-1}^2} \end{array} \right)$$

Then making use of this function, the currents corresponding to the Reverse (signal measured at the input port) and Forward (signal measured at the output port) PIM products can be evaluated as $R_2 I_{q,p,1}(0)$ and $R_2 I_{q,p,1}(l)$, respectively.

III. Nonlinear Resistance for a Microstrip Line

The obtained solution allows modeling of PIM, provided the macroscopic nonlinear parameter R_2 remains constant in the simulation. This is not always the case, since variation of the line width, for example, changes the surface current density and, hence, the nonlinear resistance. In order to address this problem, the relationship between nonlinear resistance and resistivity should be established.

Let us represent a third order microscopic nonlinearity by means of Ohm's law and consider the one-dimensional case, which allows us to use the magnitudes of the vectors directly

$$E = \rho_0 J + \rho_2 J^3 \tag{8}$$

where E – electric field, J – surface current, ρ_0 – linear surface resistivity of the metal, ρ_2 – nonlinear surface resistivity.

In order to relate the current density to the full current on microstrip line, we employ the approximation of planar waveguide with magnetic walls [9]. This model suggests the current density as follows:

$$J = \frac{I}{w_{eff}} \tag{9}$$

where w_{eff} – effective width of the microstrip line. The closed form approximation for w_{eff} has been evaluated by conformal mappings [10]:

$$w_{eff} = w + \frac{4h}{\pi}\ln 2 + \frac{2h}{\pi\varepsilon_r}\left(1 + \ln\left(4 + \frac{2\pi w}{h}\right)\right) \qquad (10)$$

where w, h and ε_r are the strip width, substrate height and dielectric constant of the microstrip line respectively. The strip thickness can be incorporated in (10) by using the width corrections given in [9].

Now, substituting (9) into (8) and recalling that $E = -\frac{dU}{dx}$, we arrive to the reduced telegrapher's equation:

$$-\frac{dU}{dx} = \rho_0 \frac{I}{w_{eff}} + \rho_2 \frac{I^3}{w_{eff}^3} = R_0 I + R_2 I^3$$

Whence we obtain

$$R_2 = \frac{\rho_2}{w_{eff}^3} \qquad (11)$$

Thus the macroscopic nonlinear resistance R_2 given by (11) takes into account the effect of the microstrip line parameters as well as the intrinsic nonlinearity.

IV. Model Verification and Numerical Results

A. Model Verification

Verification of the model has been carried out by comparison of the simulated results with the experimental results [11] where PIM dependence on the length of a line with distributed nonlinearity was measured by applying pieces of office tape with nonlinear powder to the line.

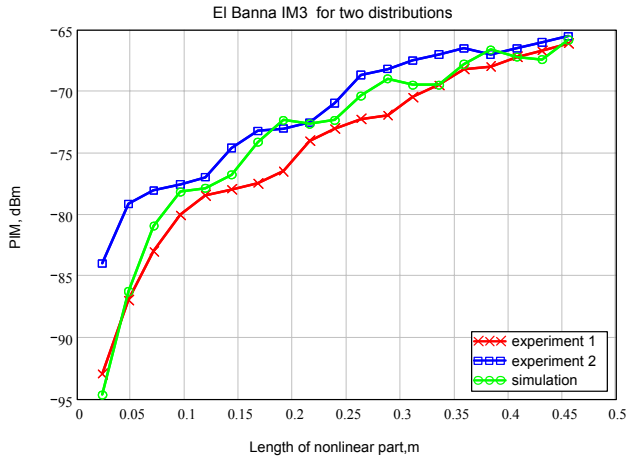

Fig. 2. Forward PIM for microstrip line with artificial distributed nonlinearity.

The pieces were 2.4cm long each. Using 19 pieces, PIM was measured on the lines with nonlinear section up to 45.6cm. Two experiments have been made by mixing and reapplying pieces to provide different distributions of the nonlinearity. The carriers' power was 2x34dBm at the frequencies in GSM band.

The experimental and simulated results are presented in Fig. 2 and Fig. 3. The nonlinear parameter R_2 = 0.05 $\Omega A^{-2}m^{-1}$ has been estimated by fitting the measured level of Forward PIM. The R_2 value is rather high for an ordinary microstrip line [6], but it still satisfies the criteria of weak nonlinearity. The reflection coefficients for source and load have been chosen equal -0.14, which is fairly close to the experimental measurements without the tape pieces.

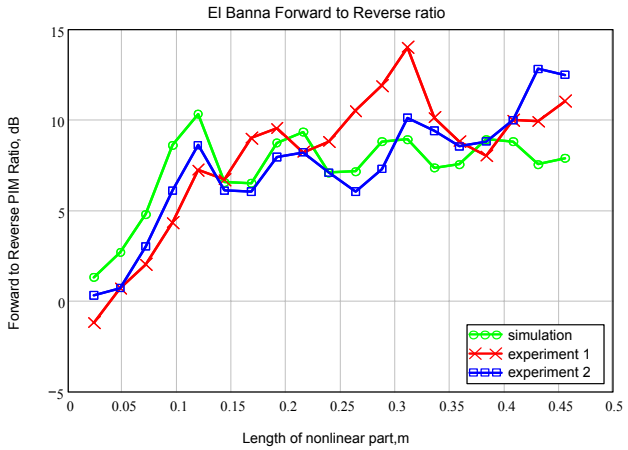

Fig. 3. Forward to Reverse PIM ratio for microstrip line with artificial distributed nonlinearity.

The comparison of the measurements and simulations demonstrates very good agreement for both Forward PIM and Forward to Reverse ratio (FRR). It was also observed, that phase of the reflection coefficient plays an important role in formation of Reverse PIM.

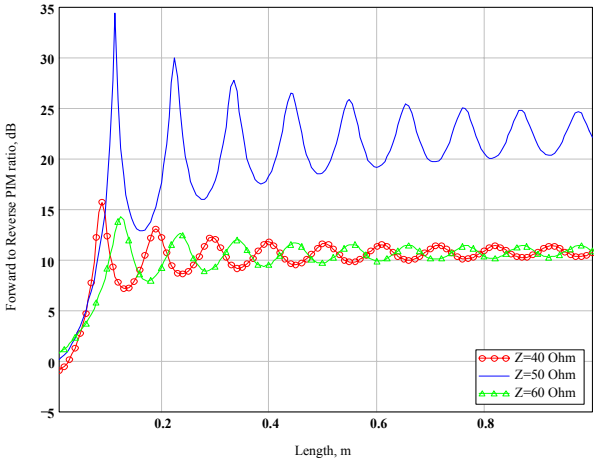

Fig. 4. Forward to Reverse PIM ratio for the line with the matched source and load of impedance Z.

The simulated FRRs for the line with matched source and different load impedances are shown in Fig. 4 for the 50Ω microstrip line with width W = 4.43mm, substrate height H = 1.57mm, substrate dielectric constant ε_r = 2.5, loss tangent $tan\delta$ = 0.0019 and copper thickness T = 35μm. The positions of maxima for the 40Ω load are well correlated with the minima for the 60Ω load that is related to the opposite signs of the reflection coefficients with almost equal magnitudes. The FRR for the matched load reaches up to 35dB, depending on the line length. Forward PIM for the line was measured in [6] as -115dBm for 917mm long line. Hence, the nonlinear resistivity ρ_2=$10^{-11}\Omega A^{-2}m$ was fitted to provide the same PIM level. Further, in the paper, all the simulations are presented for 2x43dBm input power level in the GSM band.

B. *Effect of microstrip line width on PIM*

In this section, we theoretically analyse effect of microstrip line width on PIM characteristics. Obviously, variation of the parameter leads to the change of the wave impedance and, therefore, the current density on the traces at the same power of carriers. Furthermore, this leads to mismatch of the load and source, which strongly influences PIM performance.

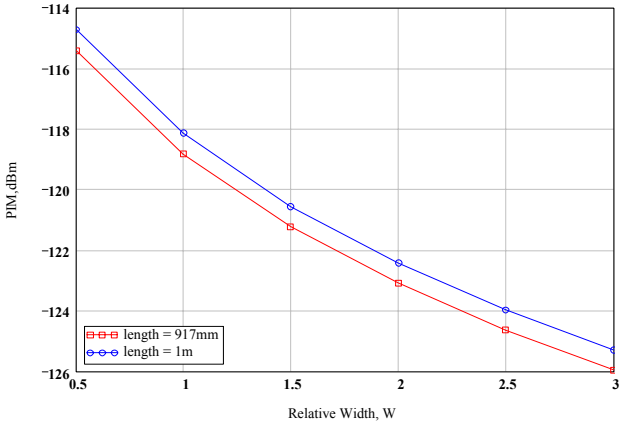

Fig. 5. Forward PIM versus relative width of the strip for two lines of different length.

To deliver all the power into the line, good source and load matching has to be ensured. Fulfilling this condition, the reflection coefficient from the load and source has been set at the level -40dB that provides good matching of the line despite its impedance variation.

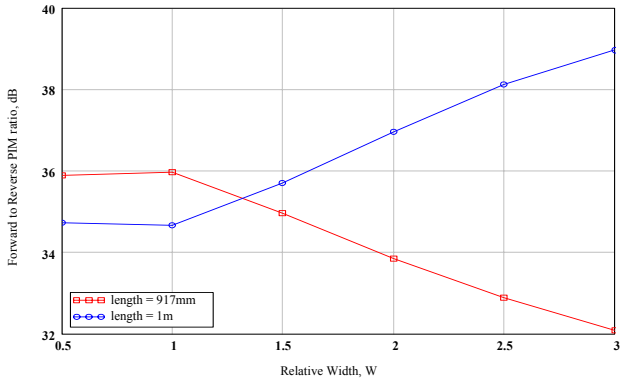

Fig. 6. Forward to Reverse PIM ratio versus relative width of the strip for two lines of different length.

Fig. 5 shows Forward PIM for two lines of lengths 917mm and 1m. Increase of the strip width, normalized to the nominal W = 4.43mm, results in monotonous decrease of Forward PIM on both lines. The experimental studies [12] also report smaller PIM level on the lines with wider strips. It is important to note that the use of R_2 in the form (11) is essential to ensure physically meaningful results. Without proper account of R_2 dependence on width, the simulated PIM level would grow due to increase of the full current magnitude.

While Forward PIM levels only slightly differ for these two line lengths in Fig. 5, the respective FRRs vary significantly as shown in Fig. 6. FRR for the 917mm line falls with the width, but rises on 1m line. This can be attributed to the strong dependence of FRR on the line length as has been demonstrated earlier in Fig. 4. Analysis of the Forward PIM and FRR shows that both Reverse and Forward PIM decrease with the line width, but the rate of decrease of Reverse PIM may be slower or faster at different line lengths.

V. Conclusions

The theory of PIM generation on printed transmission lines has been proposed. The new model for a terminated section of the transmission line with distributed nonlinear resistance has been developed and verified against the experimental data. The closed form relation between the macroscopic nonlinear resistance and microscopic nonlinear surface resistivity has been obtained. The presented theory provides an insight into the mechanisms of PIM generation and explains the fall of PIM level on wider strips observed experimentally in [12].

Acknowledgment

The work is supported by EPSRC grant EP/C00065X/1.The authors are grateful to Professor V. Fusco and Dr D. Linton from Queen's University of Belfast and Dr M. Shahabadi from University of Tehran for the stimulating discussions. The authors appreciate the generous help of Taconic ADD and assistance of Trackwise Ltd., Racal Antennas Ltd., Rosenberger Hochfrequenztechnik GmbH & Co. KG, Castle Microwaves, and PCTEL Ltd.

References

[1] A.P. Foord and A.D. Rawlins, "A study of passive intermodulation interference in space RF hardware," (ESTEC contract 111036 final report), University of Kent at Canterbury, May 1992.

[2] C. F. Hoeber, D. L. Pollard, and R. R. Nicholas, ''Passive intermodulation product generation in high power communication satellites,'' in *Proc. Communication Satellite Systems Conf.*, San Diego, CA, Mar. 1986, pp. 361-374.

[3] S Hienonen, "Studies on microwave antennas: passive intermodulation distortion in antenna structures and design of microstrip antenna elements," Dissertation for the Degree of Doctor of Science in Technology, Helsinki University of Technology, Finland, March 2005.

[4] A.G. Schuchinsky, J. Francey, and V.F. Fusco, "Distributed sources of passive intermodulation on printed lines," in *Proc. 2005 IEEE AP-S/URSI Symposium*, USA, vol.4B, 2005, pp.447-450.

[5] J. Francey, "Passive intermodulation study," Taconic ADD Tech. Rep., April 2002, www.taconic-add.com

[6] D.E. Zelenchuk, A.P. Shitvov and A.G. Schuchinsky,"Effect of laminate properties on passive intermodulation generation",. in *Proc. LAPC2007,* Loughborough, UK, 2007, pp.169-172.

[7] J.V.S. Perez, F.G. Romero, D. Ronnow, A. Soderbarg, and T. Olsson, "A microstrip passive intermodulation test set-up; comparison of leaded and lead-free solders and conductor finishing," in *Proc. MULCOPIM 2005*, ESTEC, Noordwijk, The Netherlands.

[8] R. E. Collin, *Foundation for Microwave Engineering*, 2nd Ed., McGraw-Hill, 1992.

[9] R. K. Hoffmann, *Handbook of Microwave Integrated Circuits*, Artech House, 1987.

[10] A.G. Schuchinsky, "Synthetic CAD models for structures with right-angle conductor wedges (conformal mapping approach)", in *Proc. 32nd European Microwave Conf.*, Milan, Italy, 2002, v.1, pp. 343-346.

[11] B. El Banna, "Passive intermodulation from printed circuit boards," M. Eng. Thesis, Royal Institute of Techn., Stockholm, Sweden, June, 2006.

[12] N. Kuga and T. Takao, "Passive intermodulation evaluation of printed circuit board by using 50Ω microstrip line," in *Proc. APMC 2004*, New Delhi, India.